Journal of Visualized Experiments

Measuring the Time-evolution of Nanoscale Materials with Stopped-flow and Small-angle Neutron Scattering

--Manuscript Draft--

Article Type:	Invited Methods Collection - JoVE Produced Video
Manuscript Number:	JoVE62873R2
Full Title:	Measuring the Time-evolution of Nanoscale Materials with Stopped-flow and Small-angle Neutron Scattering
Corresponding Author:	Elizabeth Kelley National Institute of Standards and Technology Gaithersburg, MD UNITED STATES
Corresponding Author's Institution:	National Institute of Standards and Technology
Corresponding Author E-Mail:	egk@nist.gov
Order of Authors:	Elizabeth Kelley
	Michael Nguyen
	Drew Marquardt
	Brian Maranville
	Ryan Murphy
Additional Information:	
Question	**Response**
Please specify the section of the submitted manuscript.	Engineering
Please indicate whether this article will be Standard Access or Open Access.	Standard Access ($1400)
Please indicate the **city, state/province, and country** where this article will be **filmed**. Please do not use abbreviations.	Gaithersburg, Maryland, United States
Please confirm that you have read and agree to the terms and conditions of the author license agreement that applies below:	I agree to the Author License Agreement
Please provide any comments to the journal here.	
Please confirm that you have read and agree to the terms and conditions of the video release that applies below:	I agree to the Video Release

TITLE:

Measuring the Time-evolution of Nanoscale Materials with Stopped-flow and Small-angle Neutron Scattering

AUTHORS AND AFFILIATIONS:

Elizabeth G. Kelley[1], Michael H. L. Nguyen[2], Drew Marquardt[2,3], Brian B. Maranville[1], Ryan P. Murphy[1]

[1]NIST Center for Neutron Research, National Institute of Standards and Technology, Gaithersburg, Maryland, USA
[2]Department of Chemistry and Biochemistry, University of Windsor, Windsor, Ontario, Canada
[3]Department of Physics, University of Windsor, Windsor, Ontario, Canada

Email addresses of co-authors:

Michael H. L. Nguyen (nguye117@uwindsor.ca)
Drew Marquardt (drew.marquardt@uwindsor.ca)
Brian B. Maranville (brian.maranville@nist.gov)

Corresponding authors:

Elizabeth G. Kelley (egk@nist.gov)
Ryan P. Murphy (ryan.murphy@nist.gov)

KEYWORDS:

Small-angle neutron scattering (SANS), time-resolved scattering, stopped-flow mixing, molecular exchange kinetics, lipid nanoparticles, lipid membranes, vesicles, structural evolution

SUMMARY:

This protocol presents the use of a stopped-flow sample environment to quickly mix multiple liquid solutions *in situ* during a small-angle neutron scattering measurement and to study kinetic processes on nanometer length scales and second time scales.

ABSTRACT:

This paper presents the use of a stopped-flow small-angle neutron-scattering (SANS) sample environment to quickly mix liquid samples and study nanoscale kinetic processes on time scales of seconds to minutes. The stopped-flow sample environment uses commercially available syringe pumps to mix the desired volumes of liquid samples that are then injected through a dynamic mixer into a quartz glass cell in approximately 1 s. Time-resolved SANS data acquisition is synced with the sample mixing to follow the evolution of the nanostructure in solution after mixing.

To make the most efficient use of neutron beam time, we use a series of flow selector valves to automatically load, rinse, and dry the cell between measurements, allowing for repeated data collection throughout multiple sample injections. Sample injections are repeated until sufficient neutron scattering statistics are collected. The mixing setup can be programmed to systematically

vary conditions to measure the kinetics at different mixing ratios, sample concentrations, additive concentrations, and temperatures. The minimum sample volume required per injection is approximately 150 µL depending on the path length of the quartz cell.

Representative results using this stopped-flow sample environment are presented for rapid lipid exchange kinetics in the presence of an additive, cyclodextrin. The vesicles exchange outer-leaflet (exterior) lipids on the order of seconds and fully exchange both interior and exterior lipids within hours. Measuring lipid exchange kinetics requires *in situ* mixing to capture the faster (seconds) and slower (minutes) processes and extract the kinetic rate constants. The same sample environment can also be used to probe molecular exchange in other types of liquid samples such as lipid nanoparticles, proteins, surfactants, polymers, emulsions, or inorganic nanoparticles. Measuring the nanoscale structural transformations and kinetics of exchanging or reacting systems will provide new insights into processes that evolve at the nanoscale.

INTRODUCTION:

Small-angle neutron scattering (SANS) provides a unique way to measure the sizes, shapes, interactions, and organization of various materials on length scales from ≈1 nm to ≈100 nm[1-3]. Recent instruments, including VSANS (very small-angle neutron scattering) instruments with focusing mirrors, push the limits toward measuring even larger length scales up to ≈1000 nm[4,5]. In general, the unique scattering contrast inherent to neutron scattering methods offers several advantages in measuring the time-evolution of nanoscale structures, such as the aggregation of components in pharmaceutical formulations[6], crosslinking and gelation reactions in polymer systems[7,8], *in meso* crystallization of membrane proteins[9,10], degradation and unfolding of proteins[11,12], and growth of silica-based materials[13-15]. The unique scattering contrast makes time-resolved SANS (TR-SANS) a useful complement to other stopped-flow-based measurements.

Stopped-flow mixing methods often are implemented in small-angle X-ray scattering (SAXS)[16-21], fluorescence spectroscopy[22-26], and light scattering[27-32] experiments to study kinetic processes on the millisecond time scales. An important difference between SANS and SAXS is that neutron scattering is a nondestructive characterization technique, and as such, SANS can be used to measure the same sample for hours or even days without ionizing radiation damage to the sample, which can happen during higher-flux X-ray scattering experiments[33]. As repeated SANS measurements will not alter the chemical structure of the probe molecule or sample, the time-evolution can be studied without effects of photobleaching, for example, which can complicate kinetics measurements that rely on fluorescence[23,24]. Moreover, SANS can be used to measure highly concentrated and optically opaque samples that are often difficult to characterize with light-based techniques such as dynamic light scattering.

In addition to providing structural information on the nanoscale, SANS can be used to probe the local composition of these structures through the variation in neutron scattering length density contrast. The scattering length density (SLD) of different elements varies randomly across the periodic table and varies with different isotopes of the same element. A commonly exploited example is hydrogen (^{1}H or H) and deuterium (^{2}H or D), which have vastly different neutron

scattering lengths. Therefore, hydrogen-rich materials, such as surfactants, lipids, proteins, RNA, DNA, and other polymers, can be distinguished from deuterated solvents using SANS without significantly changing the physical properties of the system. However, it is important to note that H/D exchange can affect the density, hydrogen-bonding, and phase transition temperatures in the sample. Nevertheless, the unique sensitivity of SANS to hydrogen-rich materials is especially useful in soft matter research where the samples of interest have lower scattering contrast and signal in X-ray-based techniques such as SAXS. Isotopic substitution also makes SANS a powerful tool for studying molecular exchange kinetics in hydrogen-rich materials by simply mixing H-labeled and D-labeled molecules. Isotopic substitution is particularly useful in systems where bulky fluorescent dyes are larger than the surfactant or lipid molecules of interest and can influence the exchange kinetics[34,35].

Time-resolved SANS measurements are advantageous because the measured intensity is a function of time, length scale, and SLD contrast. As such, TR-SANS experiments can be designed to probe the time-dependent changes in the spatial distributions and the compositions of the samples. These unique advantages of SANS have led to important insights into kinetic processes in many soft material systems such as surfactants[36-38], emulsions[39-41], lipids[34,42-50], and polymers[51-62]. Most TR-SANS studies have focused on time scales of minutes to hours. However, many kinetic processes of interest occur on the second time scale and are essential for understanding the underlying mechanisms. Capturing these early time points requires that the solutions be rapidly mixed and measured *in situ*, in which the mixing is synced with data collection during stopped-flow light scattering[27-32], fluorescence[22-26], and X-ray[16-21] experiments. This work describes the use of a sample environment designed to rapidly mix multiple liquid samples and inject the mixture into a quartz glass cell for TR-SANS measurements. The mixing device is an adaptation of the recently developed capillary rheoSANS device[63] and uses multiple syringe pumps and valves to control the sample mixing and to automate cell cleaning. By connecting syringe pumps to a series of flow selector valves, multiple inlet streams can be repeatedly mixed, measured, rinsed, and dried to facilitate TR-SANS measurements on the seconds time scale.

The current procedure assumes that the samples of interest have been identified and prepared. We focus on the *in situ* mixing setup and methods to collect TR-SANS data. Neutron scattering data were collected on the VSANS instrument at the NIST Center for Neutron Research (NCNR); however, the procedure should be applicable to other SANS instruments. Readers interested in implementing similar protocols on other SANS instruments should consult with the local instrument scientists to determine the optimal instrument configuration to maximize neutron flux at the desired length scale and time scale most relevant to the kinetic processes of interest. The data presented here were collected using the high flux 'white beam' configuration on VSANS to maximize neutron counts at the loss of spatial resolution. The detector carriages were positioned to cover a range of scattering vectors (q), 0.005 $Å^{-1}$ < q < 0.5 $Å^{-1}$, corresponding to length scales of ≈130 nm to ≈13 nm[5]. The scattering vector is defined as $q = 4\pi/\lambda \sin(\theta/2)$ in which λ is the neutron wavelength, and θ is the scattering angle.

The stopped-flow mixing device used for the TR-SANS measurements consists of multiple pumps, rinsing syringes, sample syringes, flow selectors, dynamic mixer, sample cell, and mixed sample

container, as shown in **Figure 1**. All sealed fluid paths are located inside an air-conditioned enclosure, which includes the syringes, valves, connection tubing, dynamic mixer, and sample cells. A programmable thermoelectric air conditioner is used to control the enclosure temperature in the range from 10 °C to 50 °C within ±1 °C. Note that some of the enclosure insulation was removed to show the working parts of the device. The main mixing device enclosure is positioned on a translational stage on the NG3 VSANS beam line at the NCNR. The enclosure position is adjusted using the translation stage to position the sample cell in the path of the neutron beam (yellow dashed line).

[Place **Figure 1** here]

The device depicted in **Figure 1** is configured with two sample syringes, two rinsing syringes, and one sample cell. Corresponding flow diagrams for the different steps of the protocol are illustrated in **Figure 2**. The desired volumes of the two different samples are injected into the mixer and the sample cell (**Figure 2A**). Once the sample cell is filled, the Inlet Switch Valve (ISV) and Outlet Switch Valve (OSV) are closed to isolate the sample cell from the dynamic mixer and to prevent sample back diffusion into the cell during TR-SANS data collection (**Figure 2B**). Before the dynamic mixer, the connection tubing varies in length from 10 cm to 1 m and does not affect the mixing delay time. However, tubing connections between the dynamic mixer and the sample cell will affect the mixing delay time and the required sample injection volume. Precut stainless steel tubing with 0.04 inch (1 mm) inner diameter and 100 mm length are used to connect the dynamic mixer, the Mixer Selector Valves (MSV1 and MSV2), and the ISV and OSV. Fluorinated tubing with 1 mm inner diameter and 115 mm length is used to connect the ISV and OSV (or the dynamic mixer outlet) to the sample cell. The total void volume that influences the mixing delay time includes the mixer void volume (0.15 mL), the tubing between the mixer outlet and the sample cell inlet (0.09 mL), and the sample cell volume (0.16 mL). In this example, the total void volume is 0.4 mL. The internal void volumes of valves are negligible compared to the tubing, mixer, and sample cell void volumes. For example, the employed low-pressure selector valves (0.75 mm bore diameter) contain approximate void volumes of 4 µL, while high-pressure selector valves and switch valves (0.25 mm bore diameter) contain approximate void volumes of 0.5 µL.

After the TR-SANS measurement is complete, the sample is pushed out of the cell with solvent, and rinse solvent is repeatedly pumped through the cell to remove the residual sample and clean the sample cell (**Figure 2C**). Note that the rinse syringes are connected to larger solvents reservoirs (e.g., water and ethanol) via pump selector values to ensure that adequate solvent volumes are available to clean the sample cell between measurement runs. Solvent sources, sample sources, and mixed sample containers that contain flammable liquids are positioned in a separate enclosure with no electrical equipment to eliminate all possible ignition sources. In addition, vapor-locking bottle caps are used to minimize flammable vapors and solvent evaporation. Finally, the sample cell is dried with a nitrogen gas stream to remove the residual rinse solvent (**Figure 2D**). The inlet nitrogen gas pressure to the mixer selector valve was regulated to approximately 2 bar (0.2 MPa, gauge pressure) using a manual pressure regulator located on the nitrogen gas cylinder. Once the sample cell is sufficiently cleaned and dried, a newly mixed sample is injected into the sample cell for the next measurement cycle (repeating

the mixing and injection illustrated in the flow diagram in **Figure 2A**).

[Place **Figure 2** here]

Figure 3 shows a slightly different version in which the mixing setup is configured with two separate sample cells connected to the same switch valves (**Figure 3A**). While TR-SANS data are collected in Sample Cell 1, Sample Cell 2 is rinsed (**Figure 3B**) and dried (**Figure 3C**). When the data collection is complete for Sample Cell 1, the Inlet Switch Valve directs a newly mixed sample into Sample Cell 2 for data collection (**Figure 3D**). While TR-SANS data are collected in Sample Cell 2, Sample cell 1 is rinsed and dried (**Figure 3E**). This alternating, parallel process between two sample cells minimizes the time between subsequent sample injections and maximizes the use of neutron beam time.

[Place **Figure 3** here]

A step-by-step protocol is described below for connecting the pumps and tubing lines, priming the system, rinsing and drying the sample cell, and injecting the mixed sample. Although the single-cell configuration is demonstrated for simplicity (**Figure 2**), the flexible modular setup, protocol, and scripts can be easily modified to implement more syringe pumps, valves, mixers, or sample cell configurations, such as the two-sample cell configuration shown in **Figure 3**. Representative raw neutron count rate data collected throughout mixing and cleaning injection cycles are shown in **Figure 4**, while lipid exchange kinetics measured at 3 different temperatures and the modeling of the normalized scattered intensity corresponding to the fraction of lipids exchanged are shown in **Figure 5** and **Figure 6**, respectively.

PROTOCOL:

1. Set up and initiate the stopped-flow system.

1.1. Turn on all pump power supplies and dynamic mixers using the power switch.

1.2. Initiate all pumps and valves in the stopped-flow system control graphical user interface (GUI) by entering the device configuration path and using the commands **bus=qmixbus.Bus()**, **bus.open()**, **bus.start()**, **pump=qmixpump.Pump()**, **pump.enable()**, and **valve=ViciMultiposSelector()** (see example initiation code available in an online open-source repository[64]).

1.3. Calibrate the pumps before attaching syringes using the command **pump.calibrate()**.

1.4. Confirm that the valves are initiated and move to the correct selector port on command using the command **valve.setPort()** and **valve.getPort()**.

1.5. Assign the syringe type to be used for each pump using the command **pump.set_syringe_param(A, B)**, in which **A** is the syringe barrel inner diameter (mm), and **B** is

the syringe max piston stroke distance (mm).

1.6. Connect the sample syringes to the syringe pumps.

1.6.1. After ensuring that the pumps have been calibrated, screw in clean syringe barrels to the connection at the top of the pump (syringe mount head).

1.6.2. When using glass syringes, ensure the syringe mount head is loosened before dispensing the fill volume, so that the glass syringe does not break due to excessive force from the syringe piston.

1.6.3. Screw in the syringe piston to the connection at the bottom of the pump (syringe mount tail).

1.6.4. After the syringe barrel and syringe piston are connected to the pump, dispense the fill volume of the syringe type using the command **pump.empty()**, which moves the syringe piston to the top of the syringe barrel.

1.6.5. When using glass syringes, tighten the syringe mount head after the piston stops movement.

1.7. Connect the tubing to the sample and solvent sources, syringes, valves, mixers, sample cells, and mixed sample container.

1.7.1. Connect the syringe pump tubing to the pump selector valves.

1.7.2. Connect the pump selector valve tubing to the sample sources.

1.7.3. Connect the pump selector valve tubing to the rinsing solvent sources.

1.7.4. Connect the pump selector valve tubing to the mixer selector valve tubing.

1.7.5. Connect the mixer selector valve tubing to the nitrogen gas source.

1.7.6. Connect the mixer selector valve tubing to the mixer inlets.

1.7.7. Connect the mixer outlet to the inlet switch valve.

1.7.8. Connect the inlet switch valve to the sample cell inlet.

1.7.9. Connect the sample cell outlet to the outlet switch valve.

1.7.10. Connect the outlet switch valve to the mixed sample container.

1.8. Define all tubing and valve connections made (Step 1.7) in the stopped-flow system control GUI by typing in the corresponding port number connections made to each valve (see example control code in the online open-source repository[64]).

1.9. Calculate the void volume of the tubing between the mixer inlet and sample cell outlet, which defines the minimum amount of sample needed to fill the sample cell for each measurement.

2. Load the sample.

2.1. Set the desired sample fill volume and solvent fill volume in the stopped-flow system control GUI by typing the desired numbers (see example control code in the online open-source repository[64]).

2.2. Use the **pump.aspirate()** command to pull in (aspirate) the desired sample and solvent volumes from their sources into the sample syringes through the pump selector valves.

NOTE: When first loading an empty syringe, air will be present at the top of the syringe that must be purged to prime the system with sample and solvent in step 3.

3. Prime the system.

3.1. Use the **pump.dispense()** command to push out (dispense) all air from syringes, tubing lines, and valves. Ensure that enough liquid volume is dispensed from each syringe to completely remove all air from the syringes, tubing, and valves. If air bubbles are visible inside any tubing, continue dispensing solvent or sample until the bubbles are removed.

3.2. Once air has been purged from the system, perform at least one sample injection and rinsing procedure (without neutron scattering data collected).

3.2.1. Click to select the cell labeled **Start mixing experiment** in the control GUI.

3.2.2. With this cell actively selected, click on the **Run** button (right triangle) located at the top of the control GUI, or press the **Shift** and **Enter** keys together on the keyboard.

3.2.3. Visually inspect the sample cell to confirm that air bubbles are not present.

3.2.3.1. If air bubbles are present, repeat protocol steps 3.1 and 3.2 to further purge any air from the tubing lines.

3.2.3.2. If air bubbles are not present in the sample cell, proceed to step 4 to define the remaining experiment protocol steps.

4. Define the stopped-flow mixing protocol in the program script (see code example in the online open-source repository[64]).

4.1. Enter the temperature set point of the programmable air conditioner (AC) unit that controls the temperature of the insulated enclosure surrounding the stopped-flow device.

4.1.1. While holding the **star** button on the AC control unit, press the **up** and **down** arrows to change the setpoint temperature. Alternatively, type the desired temperature setpoint in the control GUI and click on **Run**.

4.1.2. Wait for 15–30 min to allow the enclosure interior to equilibrate at the desired temperature before starting the kinetic experiments.

NOTE: The accessible temperature range is currently between 10 °C and 50 °C, and the temperature stability is $\pm$ 1 °C.

4.2. Enter all rinsing sequence steps by typing in the appropriate volumes, flow rates, times, and number of repetitions into the control GUI.

4.2.1. Define the volume of each sample to be injected, which defines the total flow rate (Q).

4.2.2. Define the volume of each solvent to be injected during the rinsing procedure.

4.2.3. Define the drying time between each rinsing substep (t_{dry}).

4.2.4. Define the number of rinsing substeps.

4.2.5. Define the different solvents for the subsequent rinsing steps.

4.2.6. Define the number of rinsing repetitions to perform after each measurement (n_{rinse}).

4.2.7. Define the time to fully dry the sample cell and mixer, providing a clean sample cell for the subsequent sample injection (t_{dry_final}).

4.3. Define all sample injection sequence steps by typing the appropriate volumes, flow rates, and times into the stopped-flow system control GUI.

4.3.1. Define the volume of each sample to be injected and the flow rate.

4.3.2. Calculate the delay time (t_{delay}) from the void volume (V_{void}) and the total flow rate ($t_{delay} = V_{void}/Q$).

NOTE: The delay time is the time needed to fill the sample cell with the mixed sample.

4.3.3. Define the desired acquisition time for the TR-SANS data such that the entire kinetic process of interest has occurred (t_{scatt}).

4.3.4. Set the wait time between the end of the scattering experiment and the beginning of the rinse cycles (t_{wait}).

NOTE: This wait time should be at least 100 s if the sample neutron transmission is to be measured before it is rinsed from the cell. The sample transmission is needed during the data processing step to reduce the data to absolute intensity.

4.3.5. Define the number of injection cycles to perform with rinsing sequences run between each injection that are defined in step 4.2 (n_{cycle}).

4.4. Calculate the total time of a single stopped-flow data collection cycle (t_{cycle}) using equation (**1**).

$$t_{cycle} = n_{rinse} \times (t_{delay} + t_{dry}) + t_{dry\_final} + t_{delay} + t_{scatt} \quad (\mathbf{1})$$

in which n_{rinse} = number of rinsing repetitions (step 4.2.6); t_{delay} = delay time of the stopped flow device (step 4.3.2); t_{dry} = drying time between each rinsing substeps (step 4.2.3); t_{dry_final} = time to fully dry the sample cell and mixer (step 4.2.7); t_{scatt} = desired TR-SANS data acquisition time (step 4.3.3)

5. Define small-angle neutron scattering parameters in the SANS instrument control GUI.

5.1.1. Determine the length scales and q-range of interest for each sample.

5.1.2. Define the instrument configuration to cover the desired q-range of interest, while maximizing the neutron flux at the sample.

5.1.3. Set the total VSANS data acquisition time in the SANS instrument control GUI to the calculated cycle time in step 4.4 (neutron scattering data acquisition time = t_{cycle}).

5.1.4. Set the sample transmission measurement time to 100 s in the SANS instrument control GUI.

5.1.5. Using the SANS instrument control GUI, turn on event mode data collection by typing **GenerateEventModeData true** in the command line.

6. Collect standard scattering measurements for data reduction before beginning the stopped-flow experiment to process the TR-SANS data.

6.1. Measure the background scattering.

6.1.1. Ensure that the local instrument shutter is closed.

6.1.2. Attach the blocked beam sample to the back of the sample aperture, secure the local instrument environment, and open the local instrument shutter.

6.1.3. Define the blocked beam scattering data acquisition time in the software, and collect blocked beam scattering data, counting for the same duration as the longest scattering data acquisition time (t_{scatt}).

6.1.4. Once the data collection is complete, close the instrument shutter, and remove the blocked beam sample from the sample aperture.

6.2. Measure the empty cell scattering.

6.2.1. Ensure that the sample cell has been thoroughly rinsed and dried.

6.2.2. Open the local instrument shutter.

6.2.3. Collect the empty cell transmission measurement for 100 s.

6.2.4. Collect the empty cell scattering measurement, counting for at least the longest acquisition time (t_{scatt}).

7. Begin the stopped-flow experiment.

7.1. Start VSANS scattering data collection in **event** mode.

7.1.1. Ensure that the local instrument area is secure and then open the local instrument beam shutter.

7.1.2. Begin SANS data collection using the SANS instrument control software on the instrument computer by dragging and dropping the desired runs into the instrument queue.

NOTE: To ensure that the earliest time points are measured, begin data collection before starting the stopped-flow mixing experiment. The data will be post-processed at a later step to account for the delay time (t_{delay}).

7.2. Start the stopped-flow mixing experiment in the control GUI.

7.2.1. Select the notebook cell labeled **Start mixing experiment** in the stopped-flow system control GUI.

7.2.2. With this cell actively selected, click on the **Run** button (right triangle) located at the top

of the stopped-flow device control program, or press the **Shift** and **Enter** keys together on the keyboard.

7.2.3. Confirm that the stopped-flow mixing protocol defined in section 4 has started operating.

7.2.4. Add the 100 s transmission measurement to the VSANS instrument queue after the scattering run using the SANS instrument control GUI.

7.2.5. Add one scattering measurement run and one transmission measurement run to the instrument queue for each remaining stopped-flow mixing cycle (n_{cycle} - 1, step 4.3.5) in the SANS instrument control GUI.

8. Process and reduce data to remove all backgrounds, correct for detector sensitivity, and correct for sample transmission.

8.1. Download the scattering data file and associated event files from the server.

NOTE: Separate detector event files will be generated after each VSANS measurement, one event file for each active detector (e.g., front, middle, and/or back detector).

8.2. Bin the scattering data to desired time bins using the command **events=Rebin(filename)** followed by the command **events.do_rebinning(timebins)**, in which the input **filename** corresponds to the name of the desired SANS data file, and **timebins** is a list of the desired time bin boundaries in seconds.

NOTE: If the input **timebins** is entered as a single number instead of a list, then the data will be binned into N number of bins with equal time widths, where N is the input **timebins** (see software scripts provided by the beamline and available online open-source repository[64]).

8.3. Reduce the binned scattering data using the software provided the beamline[65].

9. Analyze the TR-SANS data.

9.1. Calculate the process time of interest ($t_{process}$) from the measurement times using equation (**2**).

$$t_{process} = t_i - t_{stop} + t_{delay} \quad (2)$$

Where t_i is the measurement time bins starting after the flow is stopped, t_{stop} is the measurement time immediately when the flow is stopped, and t_{delay} is the delay time.

9.2. Plot the q-dependent intensity I(q) as a function of the process time using the time bins defined in step 8.2 and the calculation of $t_{process}$ in step 9.1.

NOTE: The earliest accessible process time is restricted by t_{delay}. To measure earlier process time points, increase the total flow rate (Q) or decrease the total void volume (V_{void}).

9.3. Extract the kinetic parameters of interest from the change in I(q) as a function of process time.

10. End the experiment.

10.1. Turn off the neutron beam by closing the local instrument shutter.

10.2. Perform a radiation check using a radiation monitor provided by the beamline before disconnecting any parts, tubing, or unloading any samples or mixed sample containers.

10.3. Transfer the syringes, tubing, and mixed sample container to the health physics department.

10.4. Fill out health physics forms and wait for evaluation by health physics personnel.

REPRESENTATIVE RESULTS:

The representative neutron data shown here measure lipid exchange kinetics in the presence of methyl-β-cyclodextrin (mβCD), an additive that catalyzes the lipid exchange between vesicles with the exchange rate (k_e)[66,67]. Previous fluorescence studies have shown that k_e depends on the mβCD concentration, and the half-life of the exchange process is on the order of minutes[68]. The present experiments use stopped-flow TR-SANS to measure mβCD-catalyzed lipid exchange between vesicles on the seconds time scale. Two isotopically distinct lipid vesicle populations were prepared; one vesicle population was prepared with tail-hydrogenated dimyristoylphosphatidylcholine (DMPC) lipids (H-lipid vesicles in **Figure 5**), and the other vesicle population was prepared with tail-deuterated DMPC (DMPC-d54) lipids (D-lipid vesicles in **Figure 5**). A mole fraction of 0.05 (5 mol%) of charged dimyrisotylphosphatidylglycerol (DMPG) lipid was added to both the DMPC and DMPC-d54 dry lipid powers to promote unilamellar vesicle formation[69].

Separate H-vesicles and D-vesicles solutions were prepared by hydrating the respective lipid films in a solvent containing 45% by volume heavy water (D_2O) and 55% by volume water (H_2O). The D_2O/H_2O solvent composition was calculated such that the neutron scattering length density (ρ) of the solvent matched a random mixture of the H-lipids and D-lipids ($\Delta\rho = \rho_{lipid} - \rho_{solvent} = 0$). In other words, a randomly mixed H/D-vesicle would be 'invisible' to the neutrons and generate zero coherent neutron scattering. Unilamellar vesicle solutions were prepared by freeze-thawing the solutions five times and then extruding the individual solutions through a polycarbonate filter with 100 nm diameter pores. The vesicle solutions were extruded back and forth between two syringes and the filter for a total of 31 times at 30 °C. Subsequently, a small volume of a concentrated mβCD stock solution prepared in the same D_2O/H_2O solvent mixture was added to the vesicle solutions. The final lipid concentration was 14 mmol/L (mM) and the mβCD concentration was 30 mM. The individual vesicle solutions were equilibrated for at least 30 min

with the added mβCD before the solutions were loaded into the sample syringes in the mixing device.

An example of the measured neutron count rates over multiple injection cycles is shown in **Figure 4A**. Each cycle consisted of 9 rinsing steps, 1 drying step, and 1 sample injection step. Only count rates measured on the middle detector carriage in the VSANS instrument are presented for clarity. Similar trends were found on the front detector carriage, which corresponded to data collected at larger scattering angles or higher q values. The count rate spiked with each rinsing solvent injection (solvent S1 and solvent S2) and returned to the empty cell baseline counts when the solvent was pushed out of the cell with nitrogen gas and dried. The final cell rinse was with S2, which was ethanol in this example, and the cell was dried a final time with nitrogen gas for 3 min before sample injection. Soon after the sample was injected into the cell, the neutron count rate spiked, and data were collected continuously for 5 min. The representative sample injected in the example data in **Figure 4A** was a salt buffer background. The fluctuations in measured intensity over time reflect the variations in the background neutron count rate and do not reflect a change in the average sample composition. The complete cycle of rinsing, drying, mixing, and injecting sample was repeated an additional time in the example in **Figure 4A**, where each cycle lasted for a total of 15 min.

The individual H-labeled and D-labeled lipid solutions were mixed at time t_{mix} and immediately flowed into the sample cell. The measured neutron count rate spiked and then reached a maximum value when the sample cell was filled at t_{fill}, as shown in **Figure 4B**. The elapsed time required to fill the sample cell is called the delay time t_{delay} and is given by $t_{delay} = t_{fill} - t_{mix}$. If the void volume ($V_{void}$) between the mixer and the sample cell is known and the total flow rate (Q) is known, then t_{delay} can also be calculated as $t_{delay} = V_{void}/Q$ (see protocol step 4.3.2), which is also the average residence time to enter the mixer and leave the sample cell. After reaching t_{fill}, the flow was continued at a constant flow rate to ensure that the cell had filled and reached steady-state. The flow was then immediately stopped at t_{stop}. The averaged neutron count rate remained constant as a function of measurement time between t_{fill} and t_{stop} because the flow rate through the sample cell was constant, and therefore, the sample within the neutron beam path was at steady-state. In other words, the data measured at t_{stop} correspond to the sample that has been mixed and evolved by $t_{delay} = t_{fill} - t_{mix} = V_{void}/Q$. The binned measurement times t_i collected immediately after t_{stop} are the main kinetic data of interest.

In **Figure 4C**, the neutron counts from the mixed lipid vesicles sample at three different temperatures are plotted as a function of the corrected process time scale ($t_{process}$), which is the process time of interest that has been corrected for the steady-state flow period and delay time. The process time scale was calculated by $t_{process} = t_i - t_{stop} + t_{delay}$, or equivalently, $t_{process} = t_i - t_{stop} + t_{fill} - t_{mix}$. SANS data were collected continuously in **Figure 4** in so-called **event mode**. During **event mode** data collection, each detected neutron event is recorded with a unique time stamp and its x and y location on the two-dimensional neutron detector. Event mode data can then be post-processed into the desired time bins (t_i) in **Figure 4B**.

Event mode data within the accessible process time window of interest (*i.e.,* neutron scattering

collected at each t_i after t_{stop} in **Figure 4B**) were reconstructed into a two-dimensional (2D) detector image for that time bin using protocols and scripts available in the online open-source repository[64]. Each 2D detector image was then processed using data reduction routines to subtract the different sources of background, correct for the sample transmission and detector efficiency, and azimuthally integrate the 2D detector data into intensity (I) vs. scattering vector (q) plots[65]. The data in **Figure 5** were binned into equal (3 s) time bins and are representative of the time- and length-scale-dependent information that can be gained from a TR-SANS measurement. Similar to the total raw count rate shown in **Figure 4B**, the q-dependent intensity I(q) decreases in time as the lipids in the outer leaflet exchange and mix randomly between different vesicles.

Data are presented in **Figure 5** for the lipid exchange kinetics measured at 3 different temperatures. Each plot shows the data collected for the first 15 min after mixing. The measured intensity decreases by an order of magnitude at the lowest q-values at 36 °C and 30 °C, which correspond to the lipid fluid phase. Meanwhile, the scattered intensity data change significantly slower with time at 20 °C, indicating that the outer leaflet exchange kinetics are much slower in the lipid gel phase.

The measured scattering intensity, $I(q)$, is related to the SLD contrast as $\sqrt{I(q)} \propto \Delta\rho$, in which $\Delta\rho$ is the SLD difference between the vesicle and the surrounding solvent. This average SLD contrast is directly related to the relative numbers of H-lipids and D-lipids in a vesicle at any given time. As such, the measured scattering intensity at a given time can be normalized to determine the fraction of the lipid population that has exchanged. This normalization is achieved by collecting two additional measurements, including: (1) the measured intensity I(0) at time t = 0, when there is no lipid exchange between vesicles, and (2) the measured intensity $I(\infty)$ at time t = ∞, when all of the lipids have exchanged and the populations have equilibrated. The normalized count rate, $R(t) = \left[\sqrt{I(t)} - \sqrt{I(\infty)}\right] / \left[\sqrt{I(0)} - \sqrt{I(\infty)}\right]$[42], is plotted as a function of the process time for the different temperatures in **Figure 6**. In this example, $I(t)$ is the *q-integrated* intensity at process time t (background-subtracted intensity integrated as a function of q), $I(\infty)$ is the *q-integrated* intensity at infinite time after all lipids have exchanged (which should be similar to the solvent background scattering), and $I(0)$ is the *q-integrated* intensity at time t = 0 (with no lipid exchange). $I(0)$ was measured for a mixed sample below the phase transition temperature at 20 °C where the exchange was slow, and $I(\infty)$ was measured in a separate sample that had equilibrated and fully exchanged h-lipids and d-lipids for more than 36 h at 40 °C.

The normalized count rate should decay from R(t) = 1 at process time t = 0, to R(t) = 0 at t =∞, and is directly related to SLD contrast in the sample and therefore the extent of lipid exchange[27-35]. Notice that the earliest measured R(t) data do not begin at R(t)=1 at 30 °C and 36 °C, indicating that a significant amount of lipid exchange occurred during the first 3 s after mixing, which was not experimentally accessible due to the delay time (t_{delay} = 2.4 s) of the employed stopped-flow mixing protocol. Meanwhile, the measured R(t) at 20 °C remained approximately constant for the first (2–3) minutes. For the lipid exchange kinetics measured at 30 °C and 36 °C, R(t) rapidly

decayed to ≈0.5 within 100 s, suggesting the outer leaflet lipids have completely exchanged and equilibrated within minutes. Accordingly, capturing the mβCD-catalyzed lipid exchange was made possible using stopped-flow SANS, and alternatively would be difficult to capture with manual pipette mixing. Capturing even earlier process time points (t < 3 s) will require a different mixer type with smaller void volume, smaller tubing void volumes, and higher total flow rates to decrease the delay time.

The R(t) continued to decay at longer times as the lipids flip-flop between the inner and outer leaflets. TR-SANS data for the slower flip-flop process (t > 5 min) can be collected with discrete samples mixed by hand and loaded into standard SANS sample cells, as the manual pipette mixing method takes approximately 5 min. Similarly, the lipid exchange at 20 °C in the lipid gel phase was slow enough to be mixed and measured discretely, and this measurement did not necessarily need to be studied with the stopped-flow mixing method. Measurements of kinetics processes on time scales of several minutes to hours are more efficient when the samples are mixed by manual pipette mixing. However, kinetic processes on time scales less than minutes will require this stopped-flow mixing and TR-SANS measurement procedure.

FIGURE AND TABLE LEGENDS:

Figure 1: **An example setup for combining stopped-flow mixing and small-angle neutron scattering measurements at the VSANS beamline at the NIST Center for Neutron Research.** The setup contains four syringe pumps, two syringes for solvent rinsing and two syringes for sample injection, four pump selector valves, two mixer selector valves, a dynamic mixer, a flow-through quartz cell, and a mixed sample container. Incident neutrons scatter off the mixed sample located inside the sample cell. An insulated enclosure with quartz windows and a thermoelectric air-conditioned unit are used to control the sample and all equipment at a constant temperature. The yellow dashed line shows the neutron beam path. Scale bar = 10 cm.

Figure 2: **Example flow diagram using one sample cell, two samples mixing, and two rinse solvents for cleaning.** (**A**) Mixing sample A (blue) and sample B (red), and the mixed sample (purple) is then flowed into the sample cell. (**B**) During data collection, the stopped-flow device state where the ISV and OSV switch valves are closed to isolate the sample cell and prevent back diffusion of the sample during data collection. (**C**) The cleaning steps where the sample cell is rinsed with rinse solvent from SS1 (green) after data collection. (**D**) Drying step where the sample cell is dried with nitrogen gas (orange). Abbreviations: PSV = pump selector valve; MSV = mixer selector valve; OSV = outlet switch valve; ISV = inlet switch valve; SS1 = solvent source 1; SSA = sample source A; N2 = nitrogen gas source.

Figure 3: **Example flow diagram using a two-sample cell, two samples mixing, and two rinse solvents for cleaning.** (**A**) Mixing sample A (blue) and sample B (red) and then flowing the mixed sample (purple) into sample cell 1. (**B**) The stopped-flow device state during data collection on sample cell 1 while sample cell 2 is rinsed with solvent from SS1 (green). (**C**) The stopped-flow device state during data collection on sample cell 1 while sample cell 2 is dried with nitrogen gas (orange). (**D**) Once data collection of sample cell 1 is complete, a new sample (purple) is

immediately mixed and flowed into sample cell 2. (**E**) The stopped-flow device state during data collection on sample cell 2 while sample cell 1 is rinsed with solvent from SS1 (green). While one sample cell is being measured, the other sample cell is being cleaned and dried. The stopped-flow measurement process alternates between two sample cells to minimize the time between subsequent sample mixing injections. Abbreviations: PSV = pump selector valve; MSV = mixer selector valve; OSV = outlet switch valve; ISV = inlet switch valve; SS1 = solvent source 1; SSA = sample source A; N2 = nitrogen gas source.

Figure 4: **Representative raw neutron count rate data collected throughout mixing and cleaning injection cycles.** (**A**) Example of the neutron count rate (middle detector) as a function of time during repeated rinsing sequences, drying sequence, and mixed sample injection sequence over multiple cycles. The sample in (**A**) was a salt buffer background, and the changes in intensity over time reflect the variations in the background count rate, not a change in the sample. (**B**) Monitor-normalized neutron count rate as a function of the experiment time after the injection of mixed H-lipid and D-lipid vesicles at 30 °C. The vertical dashed lines indicate the mixing start time (t_{mix}), the fill time (t_{fill}), the flow stop time (t_{stop}), and time binning region (t_i). The decay in count rate after t_{stop} is due to loss of contrast in the sample as the lipid exchange between vesicles. (**C**) Monitor normalized neutron count rates as a function of exchange process time for the first 100 s of the experiment at (blue) 20 °C, (green) 30 °C, and (red) 36 °C. The event mode data are processed into 1 s bins. Abbreviations: S1 = solvent 1; S2 = solvent 2; t_{mix} = experiment time at which the sample solutions are mixed; t_{fill} = experiment time at which the sample cell is filled; t_{stop} = experiment time at which the flow is stopped; $t_{process}$ = calculated kinetic process time of interest.

Figure 5: **Illustration of catalyzed exchange of the outer layer of lipid vesicles and corresponding changes in the scattered intensity (*I*) as a function of the scattering vector (*q*) at various temperatures.** Schematic showing lipid exchange between H-lipid and D-lipid vesicles after (**A**) initial mixing at t = 0 and (**B**) exchange of the outer layer catalyzed by methyl-β-cyclodextrin (mβCD). Reduced neutron scattering intensity as a function of scattering wave vector q. Stopped-flow mixing experiments and VSANS measurements were repeated at (**C**) 36 °C, (**D**) 30 °C, and (**E**) 20 °C. The presented data were binned into 3 s intervals over the first 10 min after mixing at each specified temperature. Error bars are the propagated uncertainty from the counting statistics and represent one standard deviation. Abbreviations: k_e = rate constant for inter-vesicle lipid exchange; mβCD = methyl-β-cyclodextrin; k_f = rate constant for inter-leaflet lipid exchange, also referred to as lipid flip-flop; I(q) = measured SANS intensity with units of cm^{-1} ; q = scattering vector.

Figure 6: **Normalized scattered intensity corresponding to the fraction of lipids exchanged that can be modeled to extract rate constants for the kinetic processes of interest.** (**A**) Lipid exchange between the outer leaflet of the vesicles occurring at time scales between 3 s and 600 s measured at (blue) 20 °C, (black) 30 °C, and (red) 36 °C. The inset in the figure zooms in on the first 60 s of the kinetic process. Error bars are the propagated uncertainty from the numerical integration of the scattering intensities and represent one standard deviation. Abbreviations: R(t) = normalized scattered intensity; $t_{process}$ = corrected process time of interest.

DISCUSSION:

The current procedure describes the mixing device and the steps to perform stopped-flow TR-SANS measurements. The device and protocol are optimized for low-viscosity liquid samples where the time scales of interest are ≈1 s to 5 min. For time scales greater than 5 min, manually mixing the samples and loading them into standard scattering cells may be easier and desirable, especially for high-viscosity samples, gels, or pastes. Accessing time scales less than 1 s requires a different mixing apparatus, lower total void volumes, and higher total flow rates to lower the delay time. It is also important to note that studying kinetic processes on these short time scales will likely require repeated sample injections to accumulate sufficient scattering counting statistics on the millisecond time scale with TR-SANS. If total sample volumes are limited, it may be desirable to use a higher flux technique, such as light scattering or X-ray scattering, which require fewer sample injections or less sample volume per injection, assuming that sufficient scattering contrast exists with light or X-ray scattering.

This modular stopped-flow SANS approach creates several key advantages and disadvantages compared to commercially available stopped-flow instruments that have been optimized for neutron scattering experiments. Key advantages include (1) alternating TR-SANS measurements between different sample cells during rinsing periods to maximize the use of neutron beam time, (2) adapting the number of syringes, syringe volumes, and mixer types for ternary sample mixing or other more complex sample mixing requirements, and (3) allowing for longer measurement periods by isolating the sample cell and eliminating back diffusion at longer time scales (>10 min). Although not implemented here, the modularity of the mixing cell design also would allow for simultaneous data collection with multiple measurement methods, such as combing SANS, UV-Vis, and fluorescence measurements[70]. Two key disadvantages of this modular setup include (1) relatively longer mixing delay times (1 s to 3 s) compared to other systems that can provide 1 ms to 100 ms delay times, and (2) smaller operating temperature range (10 °C to 50 °C) compared to other available systems that can access operating temperatures from -20 °C to greater than 80 °C.

Collecting preliminary SANS data on the samples of interest prior to performing *in situ* mixing experiments is important for collecting the best TR-SANS data, particularly in experiments designed to monitor molecular exchange kinetics, such as the example presented here. Determining accurate values of $I(0)$ and $I(\infty)$ is critical for calculating accurate values of the normalized intensity, R(t), that is modeled to extract the desired kinetic parameters. The value of $I(0)$ can be directly calculated from the measured scattering intensities of the separate H-vesicle and D-vesicle stocks, and $I(\infty)$ can be determined by preparing a separate vesicle sample prepared from a 50/50 mixture of H-lipids/D-lipids. The scattering data from these control samples can also be used to determine the optimal q-range and SANS instrument configuration for the TR-SANS measurement to maximize the signal and verify the progression of exchange kinetics during the TR-SANS experiments. If the measured intensity at the first time point after mixing does not equal the calculated $I(0)$, then faster mixing times may be needed to capture all of the processes of interest. Once the measured intensity has reached $I(\infty)$, the exchange process is complete, and the cell can be emptied and cleaned in preparation for the next

injection.

To successfully mix the liquid solutions for the TR-SANS, it is critical to ensure that all syringes, valves, and tubing lines are primed and air-free, and that all the tubing connections are secure to prevent leakage. Failing to perform these critical steps correctly could result in inaccurate mixing volumes or inaccurate absolute scattering intensities. For example, air bubbles trapped within the sample cell will decrease the measured SANS intensity because of reduced scattering volume in the neutron beam path. Alternatively, air bubbles can produce 'streaks' or 'flares' of high intensity on the detector due to beam refraction at the air-liquid interface. Unexpected changes in the measured scattering intensity over time may indicate poor sample mixing, valve leakage, air bubbles in the sample cell, or sample back-diffusion.

Collecting a transmission measurement for each sample during a TR-SANS experiment is critical for reducing the collected data to an absolute intensity. It is possible to simultaneously collect scattering and transmission data on some SANS instruments, which simplifies the overall TR-SANS data acquisition programming; however, this is not possible on all instruments, including the VSANS instrument used in this protocol. Because the sample transmission and sample scattering measurements required different instrument configurations, transmission measurements were collected at the end of the scattering measurements (protocol step 7.2.4) to ensure that scattering data were measured at the earliest time points after the sample was injected into the cell. The transmission only depends on the total elemental composition, sample path length, and the neutron wavelength. Therefore, the transmission should not change if the total elemental composition remains constant throughout the time-resolved experiment. Large differences in the transmission values between repeated runs of the same sample indicate a problem from either inconsistent mixing sample volumes, incomplete filling of the sample cell, air bubbles, or valve leakage and sample backflow during the experiment.

A unique advantage of TR-SANS is that the measured intensity is dependent on the scattering vector (q) and can be used to probe spatial changes at the nanoscale. When combined with the stopped-flow mixing device, TR-SANS can probe these nanoscale changes on the second to minute time scales, providing insights into the self-assembly and exchange of surfactants and lipids, polymer and protein aggregation upon excipient addition, nanoparticle growth and decay, or the exchange of encapsulated products in emulsions. The stopped-flow device can be configured with multiple sample syringe pumps and syringes to facilitate the mixing of two or more liquid samples. This flexibility enables the systematic investigation of additives on the kinetics of interest. For example, different volumes of a concentrated antimicrobial peptide solution could be mixed with H-vesicle and D-vesicle solutions to study the effects of peptide concentration on lipid exchange kinetics[45,46]. Additionally, because all sealed fluid paths are encased in a temperature-controlled enclosure, which includes the sample syringes, valves, mixers, and tubing, the temperature of the system can be changed to extract the thermodynamic parameters related to the kinetic processes of interest.

ACKNOWLEDGMENTS:
Access to the NG3 VSANS was provided by the Center for High-Resolution Neutron Scattering, a

partnership between the National Institute of Standards and Technology and the National Science Foundation under Agreement NO. DMR-2010792. M.H.L.N acknowledges the funding provided by Mitacs Globalink (Canada). The identification of any commercial products or trade names is to foster understanding and does not imply endorsement or recommendation by the National Institute of Standards and Technology.

DISCLOSURES:

The authors have no conflicts of interest to declare.

REFERENCES:

1 Melnichenko, Y. B., Wignall, G. D. Small-angle neutron scattering in materials science: Recent practical applications. *Journal of Applied Physics.* **102** (2), 021101 (2007).

2 Grillo, I. Small-angle neutron scattering and applications in soft condensed matter. in *Soft Matter Characterization.* Borsali, R., Pecora, R. (eds), Springer, Dordrecht (2008).

3 Hollamby, M. J. Practical applications of small-angle neutron scattering. *Physical Chemistry Chemical Physics.* **15** (26), 10566–10579 (2013).

4 Pipich, V., Fu, Z. KWS-3: Very small angle diffractor with focusing mirror. *Journal of large-scale research facilities.* **1** A31, (2015).

5 Barker, J. G. et al. in *2019 NCNR Annual Report, Special Publication (NIST SP).* Kline, S. (ed), (National Institute of Standards and Technology, Gaithersburg, MD, https://doi.org/10.6028/NIST.SP.1242 (2019).

6 Gilbert, P. H. et al. Preservative induced polysorbate 80 micelle aggregation. *Journal of Pharmaceutical Sciences.* **10** (6), 2395–2404 (2021).

7 Terashima, T. et al. In situ and time-resolved small-angle neutron scattering observation of star polymer formation via arm-linking reaction in ruthenium-catalyzed living radical polymerization. *Macromolecules.* **43** (19), 8218–8232 (2010).

8 Hashimoto, K., Fujii, K., Nishi, K., Shibayama, M. Ion gel network formation in an ionic liquid studied by time-resolved small-angle neutron scattering. *The Journal of Physical Chemistry B.* **122** (40), 9419–9424 (2018).

9 Conn, C. E. et al. Membrane protein structures in lipid bilayers; small-Angle neutron scattering with contrast-matched bicontinuous cubic phases. *Frontiers in Chemistry.* **8**, 619470 (2021).

10 van 't Hag, L. et al. Protein-eye view of the in meso crystallization mechanism. *Langmuir.* **35** (25), 8344–8356 (2019).

11 Mahieu, E. et al. Observing protein degradation by the PAN-20S proteasome by time-resolved neutron scattering. *Biophysical Journal.* **119** (2), 375–388 (2020).

12 Ibrahim, Z. et al. Time-resolved neutron scattering provides new insight into protein substrate processing by a AAA+ unfoldase. *Scientific Reports.* **7** (1), 40948 (2017).

13 Hollamby, M. J. et al. Growth of mesoporous silica nanoparticles monitored by time-resolved small-angle neutron scattering. *Langmuir.* **28** (9), 4425–4433 (2012).

14 Blin, J. L., Impéror-Clerc, M. Mechanism of self-assembly in the synthesis of silica mesoporous materials: in situ studies by X-ray and neutron scattering. *Chemical Society Reviews.* **42** (9), 4071–4082 (2013).

15 Impéror-Clerc, M., Grillo, I., Khodakov, A. Y., Durand, D., Zholobenko, V. L. New insights

into the initial steps of the formation of SBA-15 materials: an in situ small angle neutron scattering investigation. *Chemical Communications.* (8), 834–836 (2007).
16 Narayanan, T., Rüter, A., Olsson, U. SAXS/WAXS investigation of amyloid-β(16-22) peptide nanotubes. *Frontiers in Bioengineering and Biotechnology.* **9**, 654349 (2021).
17 Angelov, B. et al. DNA/Fusogenic lipid nanocarrier assembly: millisecond structural dynamics. *The Journal of Physical Chemistry Letters.* **4** (11), 1959–1964 (2013).
18 Amann, M. et al. Kinetic pathways for polyelectrolyte coacervate micelle formation revealed by time-resolved synchrotron SAXS. *Macromolecules.* **52** (21), 8227–8237 (2019).
19 Varga, Z., Wacha, A., Bóta, A. Osmotic shrinkage of sterically stabilized liposomes as revealed by time-resolved small-angle X-ray scattering. *Journal of Applied Crystallography.* **47** (1), 35–40 (2014).
20 Panine, P., Finet, S., Weiss, T. M., Narayanan, T. Probing fast kinetics in complex fluids by combined rapid mixing and small-angle X-ray scattering. *Advances in Colloid and Interface Science.* **127** (1), 9–18 (2006).
21 Grillo, I. Applications of stopped-flow in SAXS and SANS. *Current Opinion in Colloid & Interface Science.* **14** (6), 402–408 (2009).
22 Gomez-Hens, A., Perez-Bendito, D. The stopped-flow technique in analytical chemistry. *Analytica Chimica Acta.* **242**, 147–177 (1991).
23 Patel, J. T., Belsham, H. R., Rathbone, A. J., Friel, C. T. Use of stopped-flow fluorescence and labeled nucleotides to analyze the ATP turnover cycle of kinesins. *Journal of Visualized Experiments: JoVE.* (92), e52142 (2014).
24 Biro, F. N., Zhai, J., Doucette, C. W., Hingorani, M. M. Application of stopped-flow kinetics methods to investigate the mechanism of action of a DNA repair protein. *Journal of Visualized Experiments: JoVE.* (37), e1874 (2010).
25 Raney, K. D., Sowers, L. C., Millar, D. P., Benkovic, S. J. A fluorescence-based assay for monitoring helicase activity. *Proceedings of the National Academy of Sciences of the United States of America.* **91** (14), 6644–6648 (1994).
26 Roder, H., Maki, K., Cheng, H. Early events in protein folding explored by rapid mixing methods. *Chemical reviews.* **106** (5), 1836–1861 (2006).
27 Milon, A. et al. Osmotic swelling of unilamellar vesicles by the stopped-flow light scattering method. Influence of vesicle size, solute, temperature, cholesterol and three α,ω-dihydroxycarotenoids. *Biochimica et Biophysica Acta (BBA) - Biomembranes.* **859** (1), 1–9 (1986).
28 Gast, K., Nöppert, A., Müller-Frohne, M., Zirwer, D., Damaschun, G. Stopped-flow dynamic light scattering as a method to monitor compaction during protein folding. *European Biophysics Journal.* **25** (3), 211–219 (1997).
29 Antoun, A., Pavlov, M. Y., Tenson, T., Ehrenberg M, M. Ribosome formation from subunits studied by stopped-flow and Rayleigh light scattering. *Biological Procedures Online.* **6**, 35–54 (2004).
30 Zhu, Z., Armes, S. P., Liu, S. pH-Induced micellization kinetics of ABC triblock copolymers measured by stopped-flow light scattering. *Macromolecules.* **38** (23), 9803–9812 (2005).
31 Ye, J. et al. Comparative study of temperature-induced association of cyclic and linear poly(N-isopropylacrylamide) chains in dilute solutions by laser light scattering and stopped-flow temperature jump. *Macromolecules.* **41** (12), 4416–4422 (2008).
32 Liu, X. et al. Early stage kinetics of polyelectrolyte complex coacervation monitored

through stopped-flow light scattering. *Soft Matter.* **12** (44), 9030–9038 (2016).
33 Garman, E. F., Weik, M. X-ray radiation damage to biological samples: recent progress. *Journal of Synchrotron Radiation.* **26** (4), 907–911 (2019).
34 Garg, S., Porcar, L., Woodka, A. C., Butler, P. D., Perez-Salas, U. Noninvasive neutron scattering measurements reveal slower cholesterol transport in model lipid membranes. *Biophysical Journal.* **101** (2), 370–377 (2011).
35 Marquardt, D. et al. 1H NMR shows slow phospholipid flip-flop in gel and fluid bilayers. *Langmuir.* **33** (15), 3731–3741 (2017).
36 Egelhaaf, S. U., Olsson, U., Schurtenberger, P. Time-resolved SANS for surfactant phase transitions. *Physica B: Condensed Matter.* **276–278**, 326–329 (2000).
37 Tabor, R. F., Eastoe, J., Grillo, I. Time-resolved small-angle neutron scattering as a lamellar phase evolves into a microemulsion. *Soft Matter.* **5** (10), 2125–2129 (2009).
38 Gradzielski, M., Bergmeier, M., Hoffmann, H., Müller, M., Grillo, I. Vesicle gel formed by a self-organization process. *The Journal of Physical Chemistry B.* **104** (49), 11594–11597 (2000).
39 Lee, Y. -T., Li, D. S., Pozzo, L. D. Kinetic analysis of ultrasound-induced oil exchange in oil-in-water emulsions through contrast variation time-resolved small-sngle neutron scattering. *Langmuir.* **35** (47), 15204–15213 (2019).
40 Lee, Y. -T., Pozzo, L. D. Contrast-variation time-resolved small-angle neutron scattering analysis of oil-exchange kinetics between oil-in-water emulsions stabilized by anionic surfactants. *Langmuir.* **35** (47), 15192–15203 (2019).
41 Roger, K., Olsson, U., Schweins, R., Cabane, B. Emulsion ripening through molecular exchange at droplet contacts. *Angewandte Chemie International Edition.* **54** (5), 1452–1455 (2015).
42 Nakano, M., Fukuda, M., Kudo, T., Endo, H., Handa, T. Determination of Interbilayer and Transbilayer Lipid Transfers by Time-Resolved Small-Angle Neutron Scattering. *Physical Review Letters.* **98** (23), 238101 (2007).
43 Nakano, M. et al. Flip-flop of phospholipids in vesicles: kinetic analysis with time-resolved small-angle neutron scattering. *The Journal of Physical Chemistry B.* **113** (19), 6745–6748 (2009).
44 Nguyen, M. H. L. et al. Methanol accelerates DMPC flip-flop and transfer: A SANS study on lipid dynamics. *Biophysical Journal.* **116** (5), 755–759 (2019).
45 Nguyen, M. H. L. et al. Peptide-induced Lipid flip-flop in asymmetric liposomes measured by small angle neutron scattering. *Langmuir.* **35** (36), 11735–11744 (2019).
46 Nguyen, M. H. L. et al. Time-resolved SANS reveals pore-forming peptides cause rapid lipid reorganization. *New Journal of Chemistry.* **45** (1), 447–456 (2021).
47 Xia, Y. et al. Effects of nanoparticle morphology and acyl chain length on spontaneous lipid transfer rates. *Langmuir.* **31** (47), 12920–12928 (2015).
48 Xia, Y. et al. Morphology-induced defects enhance lipid transfer rates. *Langmuir.* **32** (38), 9757–9764 (2016).
49 Maric, S. et al. Time-resolved small-angle neutron scattering as a probe for the dynamics of lipid exchange between human lipoproteins and naturally derived membranes. *Scientific Reports.* **9** (1), 7591 (2019).
50 Nielsen, J. E., Bjørnestad, V. A., Pipich, V., Jenssen, H., Lund, R. Beyond structural models for the mode of action: How natural antimicrobial peptides affect lipid transport. *Journal of Colloid and Interface Science.* **582**, 793–802 (2021).

51 Willner, L., Poppe, A., Allgaier, J., Mokenbusch, M., Richter, D. TIme-resolved SANS for the determintioan of unimer exchange kinetics in block copolymer micelles. *Europhysics Letters.* **55** (5), 667 (2001).
52 Lund, R., Willner, L., Stellbrink, J., Lindner, P., Richter, D. Logarithmic chain-exchange kinetics of diblock copolymer micelles. *Physical Review Letters.* **96** (6), 068302 (2006).
53 Lund, R., Willner, L., Richter, D., Dormidontova, E. E. Equilibrium chain exchange kinetics of diblock copolymer micelles: Tuning and logarithmic relaxation. *Macromolecules.* **39** (13), 4566–4575 (2006).
54 Lund, R., Willner, L., Richter, D. Kinetics of block copolymer micelles studied by small-angle scattering methods. in *Controlled Polymerization and Polymeric Structures. Advances in Polymer Science.* Abe, A., Lee, K. S., Leibler, L., Kobayashi, S. (eds). 259, Springer, Cham, 51–158 (2013).
55 Choi, S. -H., Lodge, T. P., Bates, F. S. Mechanism of molecular exchange in diblock copolymer micelles: hypersensitivity to core chain length. *Physical Review Letters.* **104** (4), 047802 (2010).
56 Choi, S. -H., Bates, F. S., Lodge, T. P. Molecular exchange in ordered diblock copolymer micelles. *Macromolecules.* **44** (9), 3594–3604 (2011).
57 Lu, J., Bates, F. S., Lodge, T. P. Chain exchange in binary copolymer micelles at equilibrium: confirmation of the independent chain hypothesis. *ACS Macro Letters.* **2** (5), 451–455 (2013).
58 Lu, J., Bates, F. S., Lodge, T. P. Remarkable effect of molecular architecture on chain exchange in triblock copolymer micelles. *Macromolecules.* **48** (8), 2667–2676 (2015).
59 Kelley, E. G. et al. Size evolution of highly amphiphilic macromolecular solution assemblies via a distinct bimodal pathway. *Nature Communications.* **5** (1), 3599 (2014).
60 Murphy, R. P., Kelley, E. G., Rogers, S. A., Sullivan, M. O., Epps, T. H. Unlocking chain exchange in highly amphiphilic block polymer micellar systems: influence of agitation. *ACS Macro Letters.* **3** (11), 1106–1111 (2014).
61 Schantz, A. B. et al. PEE–PEO block copolymer exchange rate between mixed micelles is detergent and temperature activated. *Macromolecules.* **50** (6), 2484–2494 (2017).
62 Lantz, K. A. et al. Cavitation enables switchable and rapid block polymer exchange under high-χN conditions. *Macromolecules.* **51** (17), 6967–6975 (2018).
63 Murphy, R. P. et al. Capillary RheoSANS: measuring the rheology and nanostructure of complex fluids at high shear rates. *Soft Matter.* **16** (27), 6285–6293 (2020).
64 https://github.com/usnistgov/stopped-flow-sans.
65 Kline, S. Reduction and analysis of SANS and USANS data using IGOR Pro. *Journal of Applied Crystallography.* **39** (6), 895–900 (2006).
66 Doktorova, M. et al. Preparation of asymmetric phospholipid vesicles for use as cell membrane models. *Nature Protocols.* **13** (9), 2086–2101 (2018).
67 Huang, Z., London, E. Effect of cyclodextrin and membrane lipid structure upon cyclodextrin–lipid interaction. *Langmuir.* **29** (47), 14631–14638 (2013).
68 Sugiura, T., Ikeda, K., Nakano, M. Kinetic analysis of the methyl-β-cyclodextrin-mediated intervesicular transfer of pyrene-labeled phospholipids. *Langmuir.* **32** (51), 13697–13705 (2016).
69 Scott, H. L. et al. On the mechanism of bilayer separation by extrusion, or why your LUVs are not really unilamellar. *Biophysical Journal.* **117** (8), 1381–1386 (2019).
70 Dicko, C. et al. NUrF—Optimization of in situ UV–vis and fluorescence and autonomous

characterization techniques with small-angle neutron scattering instrumentation. *Review of Scientific Instruments.* **91** (7), 075111 (2020).
●

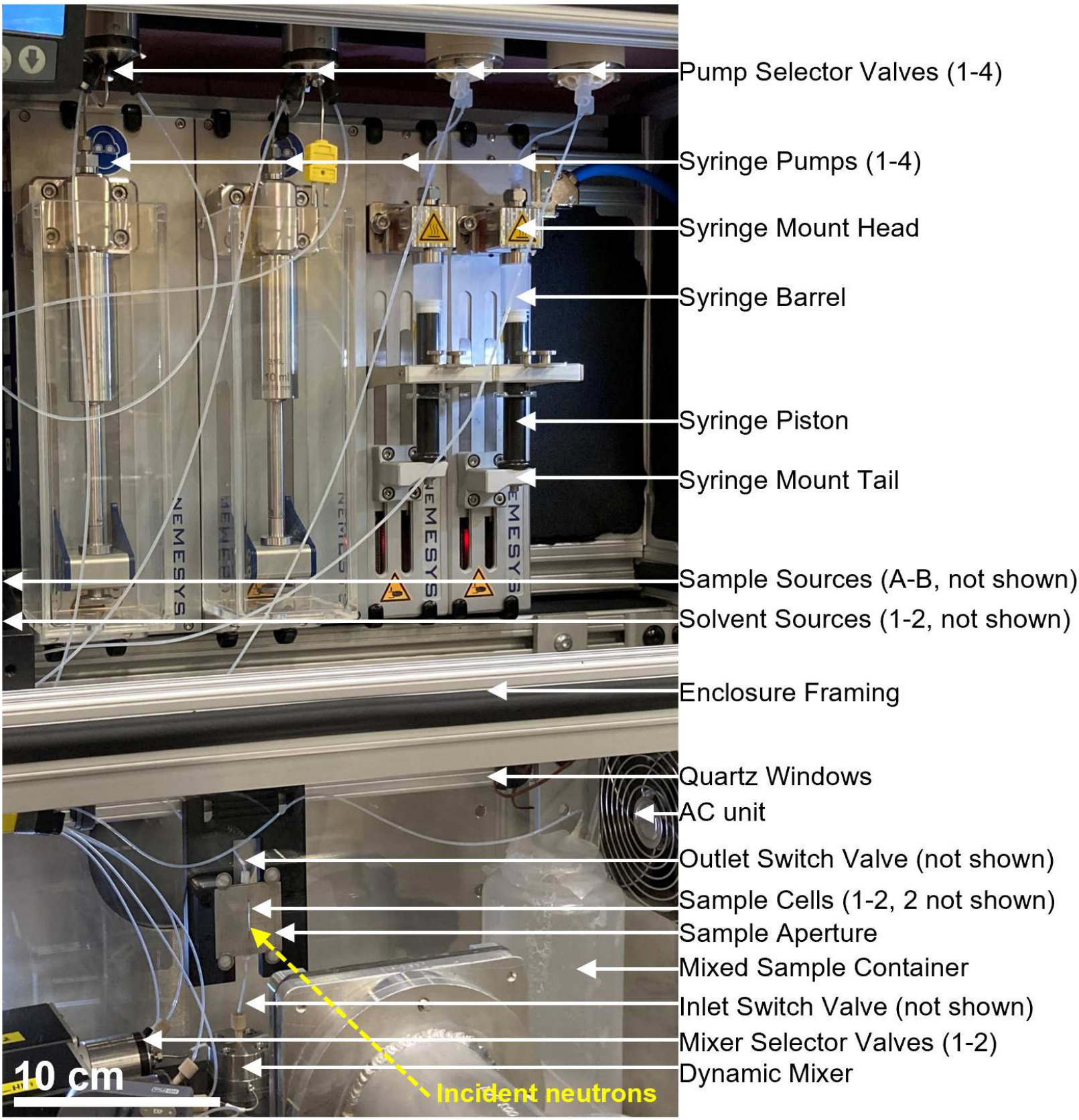

Revised Figure 2

Click here to access/download;Figure;Fig2.eps

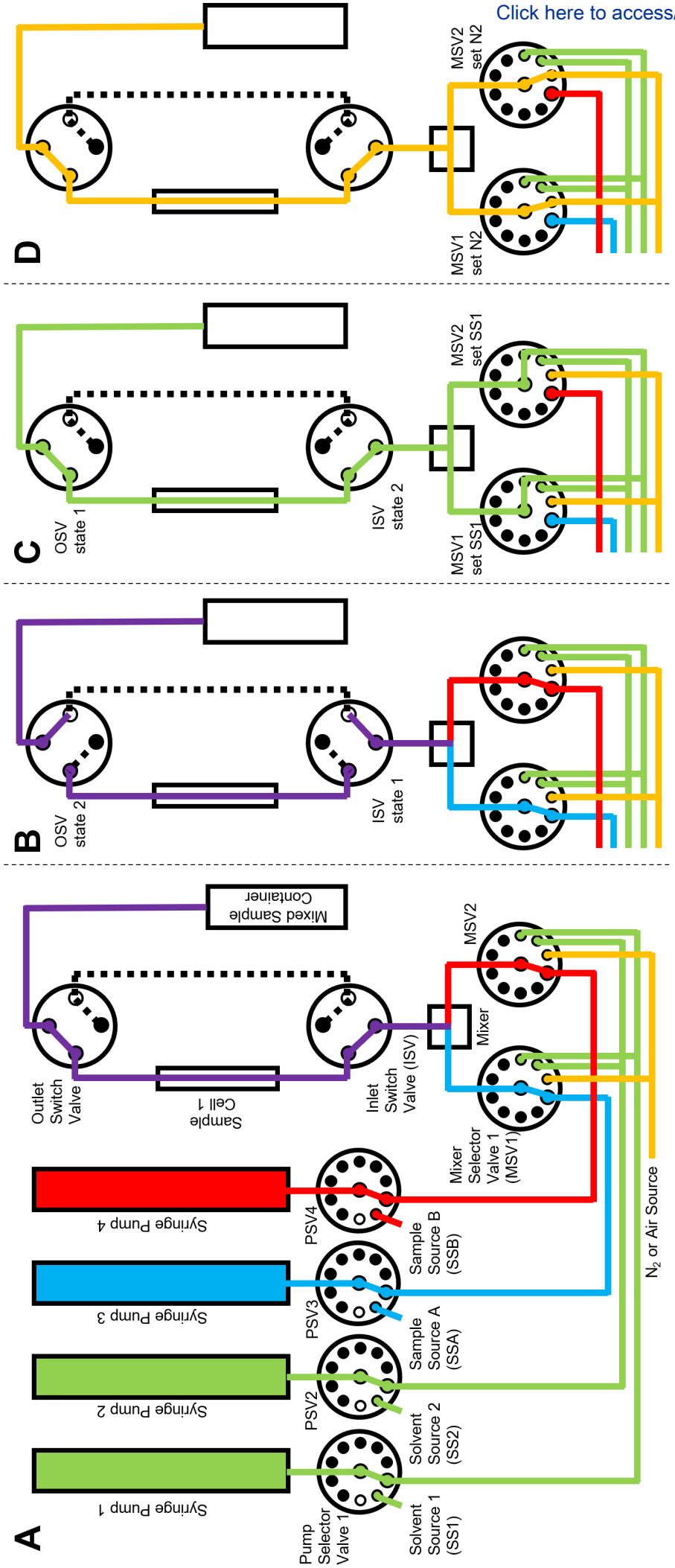

Revised Figure 3

Click here to access/download;Figure;Fig3.eps

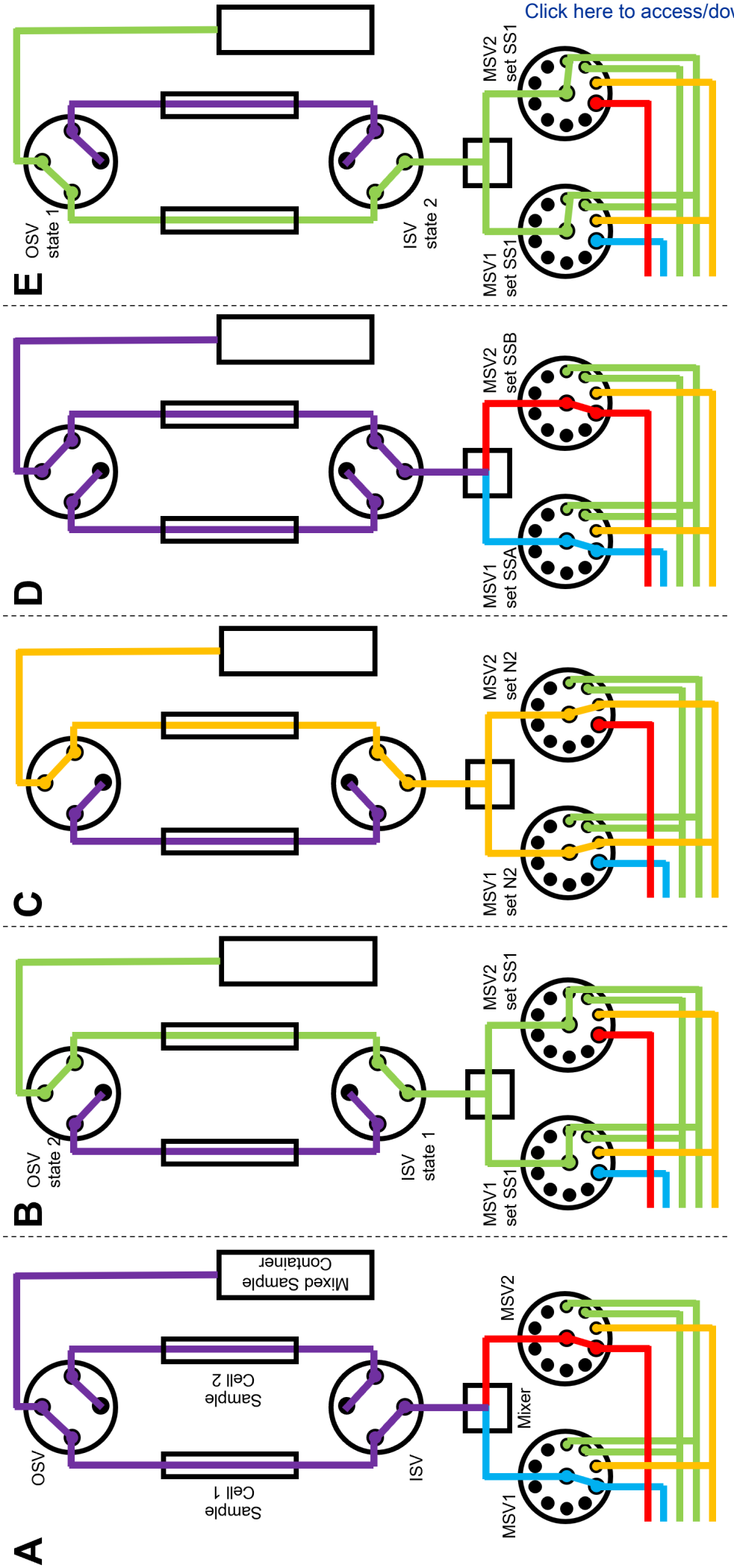

Revised Figure 4

Click here to access/download;Figure;Fig4.eps

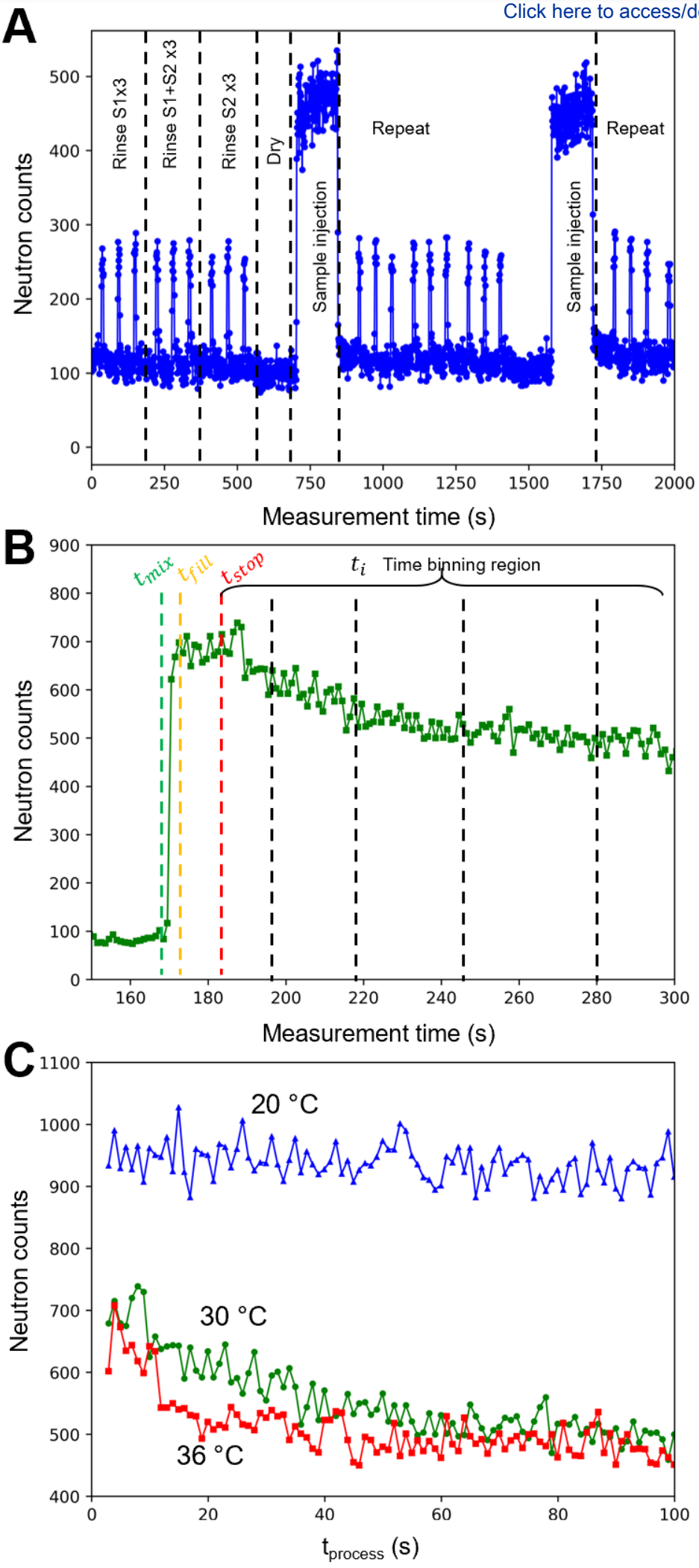

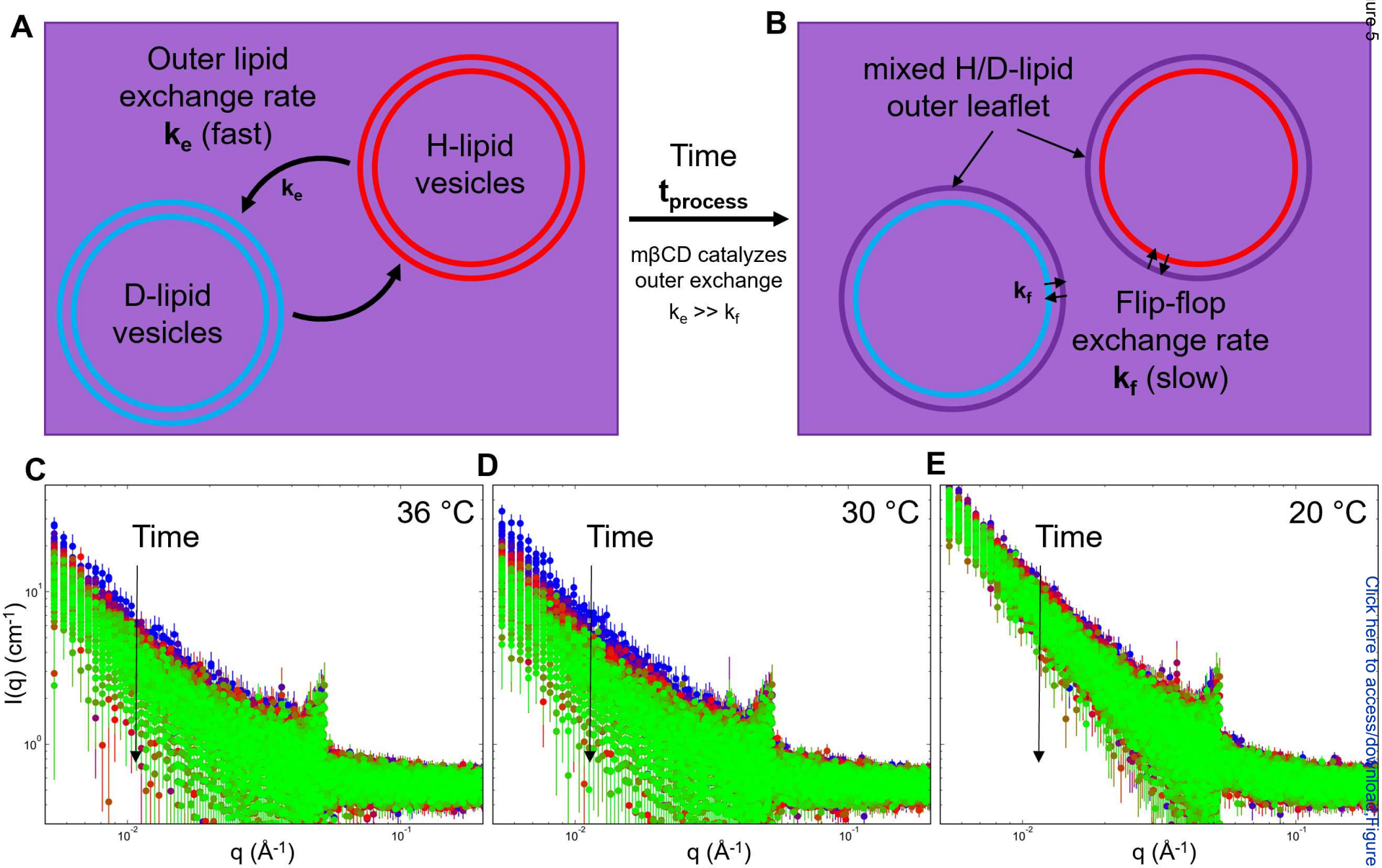

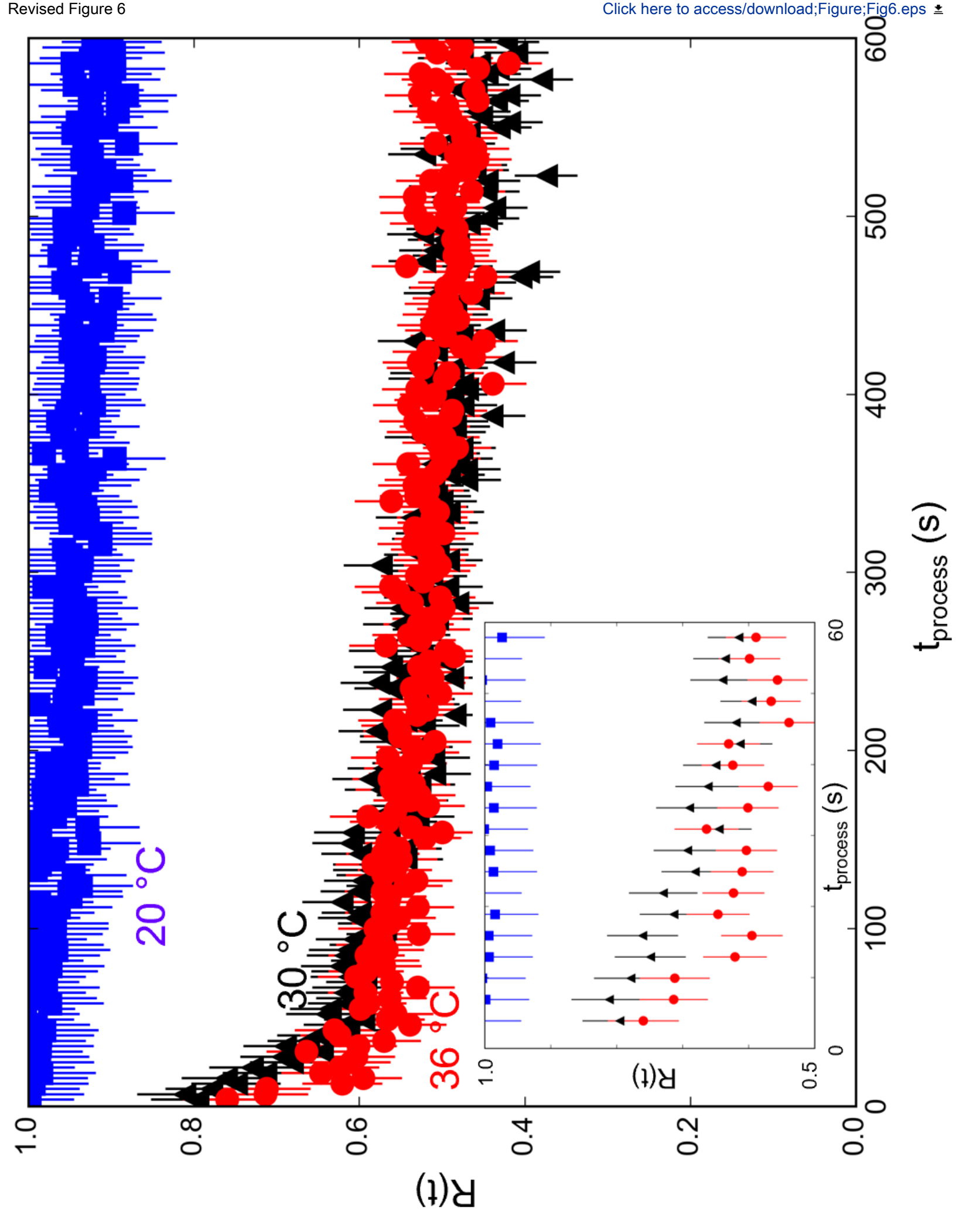

Revised Table of Materials

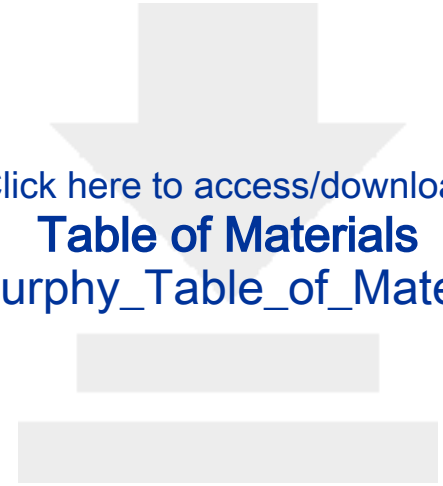

Click here to access/download

Table of Materials

Kelley-Murphy_Table_of_Materials.xlsx

We thank the editor and technical reviewers for their comments and suggestions. Our point-by-point responses to their comments are given below in blue.

Editor Comments

All requested editorial comments were implemented and are highlighted in blue text in the revised manuscript where appropriate.

Reviewer #1

(a) It would be helpful to show a scale bar in the photograph provided as Figure 1.

A scale bar has been included in the revised version of Figure 1.

(b) In general, more quantitative information would be helpful.
1. What lengths of tubing are used?

The following text regarding the lengths of tubing and associated volumes been added on pg. 4:

'Prior to the dynamic mixer, connection tubing varies in length from 10 cm to 1 m, but this tubing volume does not affect the mixing delay time. However, tubing connections between the dynamic mixer and the sample cell will affect the mixing delay time and the required sample injection volume. Pre-cut stainless steel tubing with 0.04 inch (1 mm) inner diameter and 100 mm length are used to connect the dynamic mixer and the mixer selector valves. Fluorinated tubing with 1 mm inner diameter and 115 mm length is used to connect the dynamic mixer outlet to the sample cell inlet. The total void volume that influences the mixing delay time includes the mixer void volume (0.15 mL), the fluorinated tubing between the mixer outlet and the sample inlet (0.09 mL), and the sample cell volume (0.16 mL). In this example, the total void volume is 0.4 mL.'

2. What are the volumes associated with the valves?

The following text on the volumes associated with valves has been added to pg. 4:

'The internal void volumes of valves are negligible in comparison to the tubing, mixer, and sample cell void volumes. For example, the employed low-pressure selector valves (0.75 mm bore diameter) contain approximate void volumes of 4 µL, while high-pressure selector valves and switch valves (0.25 mm bore diameter) contain approximate void volumes of 0.5 µL.'

3. What flow rates of nitrogen gas are used for drying? How is the flow regulated?
We only controlled the nitrogen gas inlet pressure. we did not control or measure the gas flow rate. We have added a statement to state the nitrogen gas inlet pressure used on pg 4.

'The inlet nitrogen gas pressure to the mixer selector valve was regulated to approximately 2 bar (0.2 MPa, gauge pressure) using a manual pressure regulator located on the of the nitrogen gas cylinder.'

(c) Figure 2 shows connection to either nitrogen or air. Are any safety protocols/procedures in place to avoid dangerous mixtures of flammable solvent and air? The flash point of pure ethanol is below the indicated measurement temperatures (often stated as 13 C).

We have added a statement to address this important safety precaution to avoid flammable solvent mixtures and electrical equipment on pg 4 in the revised text.

'Solvent sources, sample sources, and mixed sample containers that contain flammable liquids are positioned in a separate enclosure with no electrical equipment to eliminate all possible ignition sources. In addition, vapor-locking bottle caps are used to minimize flammable vapors and solvent evaporation.'

(d) Information about the temperature control would be helpful. The parts list describes a thermoelectric air-conditioner, but it is unclear whether the single enclosure includes all sample and solvent reservoirs as well as the valves, mixing chamber, measurement cell etc. What temperature stability is achieved?

We have added information about the temperature control enclosure, and we have reiterated the safety precautions above when working with flammable solvents or samples. The following text has been added to pg. 3:

'All sealed fluid paths are located inside the air-conditioned enclosure, which includes the syringes, valves, connection tubing, mixers, and sample cells.'

The temperature variability inside the enclosure is currently 1 °C and is now stated on pgs 3 and 7.

(e) At line 308 it would be useful to provide either a citation or a fuller description of 'established extrusion protocols'.

Additional information and appropriate references on the vesicle sample preparation have been included on pg. 11. The following text was added:

'*Unilamellar vesicle solutions were prepared by freeze-thawing the solutions five times and then extruding the individual solutions through a polycarbonate filter with 100 nm pore diameter. The vesicle solutions were extruded back and forth between two syringes and filter a total of 31 times at 30 °C'*

(f) The use (line 377) of a ratio defined with square roots of background subtracted count rates may not be obvious to readers. Admittedly an explanation in terms of observed scattering depending on the square of the scattering length density difference is found in the cited reference 26 but as the contrast is not expected to change linearly with time for a diffusive process, both experts and non-experts may be puzzled by the choice of function. A sentence of explanation would be helpful.

We thank the reviewer for pointing that the origins of the square root in the normalized count rates are not obvious. We have updated the text accordingly on pg 12 and the changes are highlighted in blue text in the revised manuscript.

What is the significance of using data from the middle detector (line 409) rather than all available detectors?

Data from all detectors were used in to calculate the background corrected intensity, but we chose to present the raw count rates only on the middle detector in Fig. 4 for clarity. The data on the middle detector correspond to lower q values where the scattered intensity, and thus the count rated, are higher and the changes in count rate with each injection step are more obvious. The data on the front carriage correspond to higher q and show similar trends, but the overall changes in count rate are lower because there is less scattering signal over the incoherent background.

We have also included the following text the significant of the data for the middle carriage on pg. 10:

'Only count rates measured on the middle detector carriage in the VSANS instrument are presented for clarity. Similar trends were found on the front detector carriage as well, which corresponded to data collected at larger scattering angles or higher q values.'

(g) In Figure 6 it would be interesting to show at least a typical error or uncertainty for the data that are plotted.

We have updated Figure 6 to include error bars (one standard deviation) for the kinetic parameter of interest, R(t), which was obtained by error propagation from the numeric integration of scattering intensities. Figure captions have also been updated to define the error bars in all figures.

(h) There are some typographical errors. The references should be checked carefully as errors in names may not be identified by spell-check software.

We thank the reviewer for noting these typographical errors. All have been fixed and the references have been carefully checked in the revised submission.

Reviewer #2.

1. One challenge with such time-resolved measurements is the changing transmission of the sample throughout the course of the measurement. Of course, simultaneous trans measurements are not always appropriate/possible on the instrument. I think this might be the case on VSANS and that's why the transmission is only measured at the end? Could the authors comment on this potential limitation/challenges with data reduction?

The reviewer is correct that the transmission measurements require a different instrument configuration on VSANS which is why it was measured at the end of the kinetic experiment. We have included the following paragraph about why collecting transmission data is important and how changes in transmission value between sample runs can indicate potential issues with data in the discussion beginning on pg. 15 in the revised manuscript:

'Collecting a transmission measurement for each sample during a TR-SANS experiment is critical for reducing the collected data to an absolute intensity. It is possible to simultaneously collect scattering and transmission data on some SANS instruments, which simplifies the overall TR-SANS data acquisition programming; however, this is not possible on all instruments, including the VSANS instrument used in this protocol. Because the sample transmission and sample scattering measurements required different instrument configurations, transmission measurements were collected at the end of the scattering measurements (step 7.2.4) to ensure that scattering data were measured at the earliest time points after the sample was injected into the cell. The transmission only depends on the total elemental composition, sample path length, and the neutron wavelength. Therefore, the transmission should not change if the total elemental composition remains constant throughout the course of the time-resolved experiment. Large differences in the transmission values between repeated runs of the same sample indicate a problem from either inconsistent mixing sample volumes, incomplete filling of the sample cell, air bubbles, or valve leakage and sample backflow during the experiment.'

2. It would be useful to add a short comparison with, or comment on, the commercially available stopped flow cell alternatives, e.g. the Biologic set-up with a neutron head. Such systems typically have very short delay times (<<1 s), but, the set-up here is surely far more customisable. For example, the SANS cell holder could be adapted for the inclusion of in situ characterisation techniques, e.g. spectroscopy, as well as the ability to add more cells (as described in the article) or add more syringes

As suggested, we have added a short comparison of the advantages and disadvantages of this stopped-flow setup compared to other commercially available alternatives in the revised Discussion Section beginning on pg. 14. Note we cannot state commercial equipment by name due to requirements of the journal. The following paragraph was added:

'This modular stopped-flow SANS approach creates several key advantages and disadvantages compared to commercially available stopped-flow instruments that have been optimized for neutron scattering experiments. Key advantages include (1) alternating TR-SANS measurements between different sample cells during rinsing periods to maximize the use of neutron beam time, (2) adapting the number of syringes, syringe volumes, and mixer types for ternary sample mixing or other more complex sample mixing requirements, and (3) allowing for longer measurement periods by isolating the sample cell and eliminating back diffusion at longer time scales (>10 min). Although not implemented here, the modularity of the mixing cell design also would allow for simultaneous data collection with multiple measurement methods, such as combing SANS, UV-Vis and fluorescence measurements.[70] Two key disadvantages of this modular setup include (1) relatively longer mixing delay times (1 s to 3 s) compared to other systems that can provide 1 ms to 100 ms delay times, and (2) smaller operating temperature range (10 °C to 50 °C) compared to other available systems that can provide -20 °C to greater than 80 °C operating temperatures.'

3. Finally, I am a little lost at the definition of "process time". Unless I have misunderstood "[(t-tstop)+(tdelay-tstart)]" removes the time between delay and stop, which is the additional time while the cell is filling. The mixing process obviously begins at Tstart. I understand the scattering data from the following 60 s (while the cell is filling/reaching equilibrium) would be difficult to interpret, which I think leads to the statement "after tstop are the data of interest" and "Event mode data within the time window of interest (i.e. after tstop in Fig. 4b)", but if that else the case, why is the lowest timescale achievable from this data not ~60 s (from when the mixing started) rather than ~2 s? Please can the authors clarify.

We have renamed some 'measurement time' variables to try to improve clarity of how we translate from the measurement time (the time recorded during data acquisition) to the process time (related to the kinetic process of interest) as well as updated the description in the text on pg. 11. The 'measurement time' points are collected consecutively after the start of the SANS data acquisition, as now defined in the x-axis of Fig 3, which include the start of the mixing process (now defined as t_mix), the time when the sample cell is entirely filled with the mixed sample (now defined as t_fill), and the time at which the flow is stopped (t_stop). All measurement times after flow is stopped are defined as t_i for each arbitrary time bin.

The elapsed time required to entirely fill the sample cell is the delay time t_delay, and is given by t_delay = t_fill – t_mix. If the void volume (V_void) between the mixer and the sample cell is known and the total flow rate (Q) is known, then t_delay can also be calculated as t_delay = V_void/Q, which is also the average residence time to enter the mixer and leave the sample cell.

Given the constant flow rate, the SANS measurements are at steady-state during the measurement time period between t_fill and t_stop, which can be seen in Fig. 4 where the average neutron counts on the detector are found to be constant. To ensure this steady-state period was achieved, a total sample volume that is greater than the void volume was injected at a constant flow rate.

The sample measured at t_stop corresponds to the sample that has mixed and evolved by a process time t_delay = t_fill – t_mix = V_void/Q. Translation from the measurement time to the process time (t_process) is calculated as t_process = t_i – t_stop + t_delay, or by definition above, t_process = t_i – t_stop + t_fill – t_mix. This is the same result as before but now with different variable names to hopefully improve clarity.

The earliest measurement time point for t_i is t_stop. If you substitute t_i = t_stop above for t_process, the earliest process time is t_delay, which is 2.4 s using a total flow rate of Q = 10 mL/min and a void volume of 0.4 mL.

Reviewer #3:

Manuscript Summary:

The authors present an interesting TR-SANS method that enables the study of nanoscale kinetic processes in soft materials on timescale of seconds to minutes. This manuscript/video is interesting for a wide range of researchers in the field of soft condensed matter/polymer science and

pharmaceutical science. I therefor recommend that this paper is accepted upon minor revisions (see comments below).

Introduction:
Gives a nice overview of the application of the method described, some comments with suggestions of improvement of this section is indicated below:

- The authors discuss the benefits of neutron scattering over methods as fluorescence and light scattering. I suggest the authors also add a couple of sentences about the benefits of SANS over SAXS, especially because stopped-flow SAXS also could be used to characterize kinetic processes in nanoscale materials as the manuscript discusses, some examples: Front. Bioeng. Biotechnol. 9:654349, Phys. Chem. Lett. 2013, 4, 11, 1959-1964, Macromolecules 2019, 52, 21, 8227-8237, J. Appl. Cryst. (2014). 47, 35-40).

The suggested references have been incorporated into the introduction and are references 16 – 19 in the revised manuscript.

- As this is a method paper it could be useful to make the reader aware of issues related to influence of potential H/D isotope effects in the second paragraph of the introduction.

The reviewer raises a good point, and the following text on potential H/D isotope effects are included on pg. 2:

'However, it is important to note that H/D exchange can affect the density, hydrogen-bonding, and phase transition temperatures in the sample. Nevertheless, the unique sensitivity of SANS to hydrogen-rich materials is especially useful in soft matter research where the samples of interest have lower scattering contrast and signal in X-ray based techniques such as SAXS.'

- On line 94 where the authors indicate that the protocol could be adapted to other SANS instruments, a sentence of the instrument specifications requirements (Q- range, flux etc.) should be added.

We have included the following recommendations to users interested in implementing similar protocols on other SANS instruments on pg. 3 in the revised text:

'Readers interested in implementing similar protocols on other SANS instruments should consult with the local instrument scientists to determine the optimal instrument configuration to maximize neutron flux at the desired length scale and time scale most relevant to kinetic processes of interest. The data presented here were collected using the high flux 'white beam' configuration on VSANS to maximize neutron counts at the loss of spatial resolution. The detector carriages were positioned to cover a range of scattering vectors (q), 0.005 $Å^{-1}$ < q < 0.5 $Å^{-1}$, which corresponds to length scales of ≈ 130 nm to ≈ 13 nm.[5] The scattering vector is defined as $q = 4\pi/\lambda \sin(\vartheta/2)$ in which λ is the neutron wavelength and ϑ is the scattering angle.'

- In the paragraph started on line 377 the authors describes I(0) as the intensity at time t = 0 (with no lipid exchange), without mentioning that this can be precisely estimated by measuring the two reservoirs (h and d vesicles) separately and averaging the scattering signal. In a similar manner I(∞) can be measured directly by preparing vesicles with 50-50 h/d lipids in the same solvent. Both these references has significant influence on the R(t) curves and the authors should clarify how I(0) and I(∞) was determined in this case.

We thank the reviewer for this making suggestion on describing best practices in TR-SANS data collection. We have updated the results on pg. 12 to include how I(0) and I(∞) and were determined in the presented data. We have also included a paragraph in the revised discussion on pg. 15 describing how and why I(0) and I(∞) should be determined before beginning a TR-SANS experiment.